Gas Holdup of Rotating Foam Reactors Measured by γ-Tomography—Effect of Solid Foam Pore Size and Liquid Viscosity

Roman Tschentscher
Laboratory of Chemical Reactor Engineering, Eindhoven University of Technology, 5600 MB Eindhoven, The Netherlands

Markus Schubert and Andre Bieberle
Institute for Safety Research, Helmholtz-Zentrum Dresden-Rossendorf, 01314 Dresden, Germany

T. Alexander Nijhuis and John van der Schaaf
Laboratory of Chemical Reactor Engineering, Eindhoven University of Technology, 5600 MB Eindhoven, The Netherlands

Uwe Hampel
Institute for Safety Research, Helmholtz-Zentrum Dresden-Rossendorf, 01314 Dresden, Germany

Jaap C. Schouten
Laboratory of Chemical Reactor Engineering, Eindhoven University of Technology, 5600 MB Eindhoven, The Netherlands

DOI 10.1002/aic.13787
Published online March 12, 2012 in Wiley Online Library (wileyonlinelibrary.com).

Rotating foam reactors have already shown to give high mass transfer rates compared to stirred tank reactors. For a deeper insight into the hydrodynamics of these reactors, the hydrodynamics of rotating foam reactors were studied using γ-ray tomography. The two-phase flow through the foam block stirrer is mainly influenced by the solid foam pore size and the liquid viscosity. For low viscosity, the optimal foam block pore size was identified in the range between 10 and 20 pores per inch (ppi). With smaller pore size, the gas holdup inside the foam block strongly increases due to bubble entrapment. For higher viscosity, pore sizes larger than 10 ppi have to be used to achieve a sufficient liquid flow rate through the foam block to avoid a strong gradient over the reactor height. The effect of the hydrodynamics on the gas–liquid and liquid–solid mass transfer and the reactor performance are discussed. © 2012 American Institute of Chemical Engineers *AIChE J,* 59: 146–154, 2013
Keywords: multiphase reactors, gas holdup, tomography, solid foam

Introduction

Rotating foam reactors

Various packing types for three-phase reactors have been developed in the recent years. These are mainly based on highly porous materials. Examples of these developments are monolithic stirrers or mixers based on fiber structures.[1–4] These structures have already been applied in various fields. Examples are monolith catalyst supports in the automobile industry. Solid foams have been applied in the construction sector, because of the combination of light weight and high mechanical stability and stiffness. The high porosity makes them attractive for the use as catalyst supports. Flow through these structures shows a lower pressure drop compared with pellets or packings of spheres. Among these packings, monoliths show the lowest pressure drop. On the other hand, using solid foams and fiber packings, the struts and fibers act as static mixers for the fluid streams, which split and recombine passing the struts. This results in a good mixing of the phases and similar axial dispersion coefficients compared to conventional packings.[5,6]

Solid foams have first been applied as catalyst support in the biotechnology, where low turbulence is needed in combination with a good supply of nutrition. In the chemical technology they have been studied and applied industrially as contactors for stripping and absorption processes. Studies of the hydrodynamics have been performed for the trickle bed regime.[7,8] The use of solid foams in high gravity rotating packed bed reactors (HIGEE) has extensively been studied.[9–12] In these reactors, a donut-shaped foam block is rotated at speeds up to several thousand rotations per minute. From the stirrer shaft, liquid is sprayed onto the foam structure. The centrifugal forces drive the liquid outward. At rotational speeds up to 600 rpm, the liquid forms rivulets.[13] At rotational speeds higher than 600–800 rpm, the liquid streams are broken up into droplets and pass the foam bed

Correspondence concerning this article should be addressed to R. Tschentscher at r.tschentscher@tue.nl.

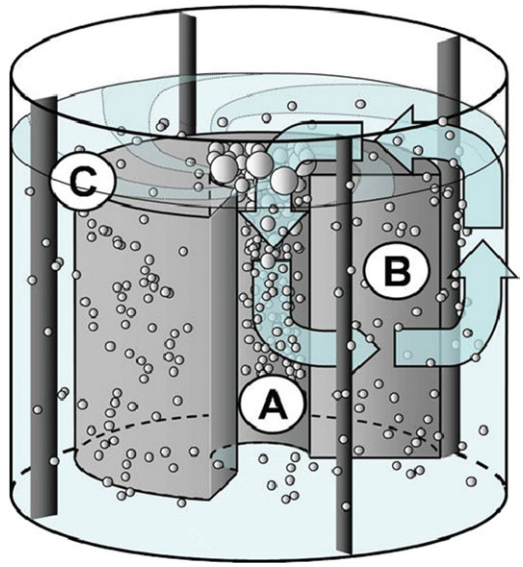

Figure 1. Principle of the foam block reactor, (Reproduced from Ref. 14, with permission from Elsevier).

Rotation induces liquid circulation as shown by the arrows. The center section (A) shows high gas holdup. In the center section, fine bubbles are created and transported through the foam structure (B). From there, the liquid–gas dispersion flows outward to section (C). Baffles improve the turbulence while the dispersion circulates back to section (A). [Color figure can be viewed in the online issue, which is available at wileyonlinelibrary.com.]

as spray. Becuase of the insufficient wetting, these reactor types have only been used industrially for stripping and absorption processes.

Previously, we have introduced a rotating foam block stirrer,[14,15] shown in Figure 1. It shows a design comparable to HIGEE-reactors but the liquid phase is used as continuum. The catalyst is immobilized on the solid foam block. In that sense, the foam block stirrer is comparable to a catalyst basket having a high bed porosity. There is no need to filter the catalyst from the reaction mixture. Other problems related to the use of slurry catalysts, such as attrition of particles and catalyst wash out do not occur. This allows a simple reuse of the catalyst. Agglomeration of particles, especially using high viscosity liquids, is precluded.

The reactor volume can be separated into different sections, each with specific hydrodynamics and gas holdup (Figure 1). Visual observations have revealed that in the center section A bubbles are trapped and broken up. Here, gas holdups higher than 50 % can be achieved. Using water, the bubbles show diameters ranging from submillimeters to a few millimeters. In the foam block section B, bubbles and liquid flow outward, passing the solid struts. The hydrodynamics in this reactor part are comparable to a trickle bed reactor working in the high interaction bubbly flow regime. The bubbles are transported into the outer reactor section C between foam block and reactor wall. From there, the dispersion is transported back into the center. Baffles disturb the flow and enhance the mixing.

Recently, we have studied the gas–liquid and liquid–solid mass transfer for these reactors.[14,15] It has been found that the rates of both mass transfer processes are high compared with a standard stirred tank system consisting of Rushton stirrer and slurry catalysts. Most importantly, the mass-transfer coefficients still increase for high power inputs above 5000 Wm^{-3} while the values using a Rushton stirrer reach a plateau.

In this article, we address the measurement of the gas holdup using γ-ray tomography. Especially the reactor volume occupied by the solid foam block is of interest as it covers a large part of the reactor volume. It is also the section where the catalyst is deposited. Previously, we have studied the gas holdup for non-Newtonian and foaming liquids.[16] We found that the surface tension mainly influences the foaming behavior of the liquid in the outer reactor sections. The viscosity has a large influence on the hydrodynamics inside the foam block, especially on the bubble entrapment inside the foam block pores. Using a carboxymethyl cellulose (CMC) solution, we have already investigated the hydrodynamics using higher viscosities, however, values only up to 67 mPa s were investigated.[16] In various industrial processes, the reactants are used directly without solvents or in high concentrations, resulting in increased viscosities. Examples for the former are the hydrogenation of fatty acids, for the latter case the glucose hydrogenation to sorbitol, where concentrations of 20–50 wt % are common. Therefore, in this work, we will study the hydrodynamics at even higher viscosities using glycerol/water mixture and pure glycerol.

The second parameter to be investigated is the foam block structure. Solid foams are available in various bed porosities and pore sizes, resulting in a wide range of specific surface areas. The foam block structure is the main parameter to tune the liquid–solid interfacial area, while keeping the bed porosity high, in our case around 0.9 $m^3_{void}\ m^{-3}_{foam}$. Regarding the catalyst one tends to use smaller foam pore sizes due to the increased liquid–solid surface area. This further allows the deposition of more catalyst per reactor volume at a constant coating thickness. Alternatively, the same amount of catalyst can be immobilized achieving a thinner coating layer. This is especially important, when mass transfer limitations inside the catalyst pores are expected. A thinner coating can then lead to an increased overall activity and a reduced formation of byproducts. The solid foam cells can be considered as small continuous stirred tank reactors (CSTRs), connected by pores. Thus, flow through a finer pore structure approaches plug-flow behavior, as smaller cells reduce the back mixing. There are, however, also disadvantages connected with having a smaller pore size. The coating of fine pores does result in an inhomogeneous coating thickness. Excess liquid after wash coating is difficult to remove, which can result in blocking of pores. Regarding the hydrodynamics, a finer pore structure and a higher specific surface area result in an increased pressure drop of through flow. In this work, the influence of the pore size is evaluated using two pore sizes of 10 and 20 pores per linear inch (ppi).

Gas holdup measurements

The gas holdup is an important hydrodynamic parameter, interlinked to the two-phase pressure drop, the flow regime and the power input. It is further correlated to the gas–liquid mass transfer rate, and by that to the reaction rate and selectivity of a chemical process. Additionally, it is an essential parameter for the reactor design. Various measurement techniques to study the gas holdup are discussed by Boyer et al.[17] Optically transparent materials and small reactor diameters can be used.[18] This increases, however, strongly the influence of the reactor wall on the bubble dynamics.

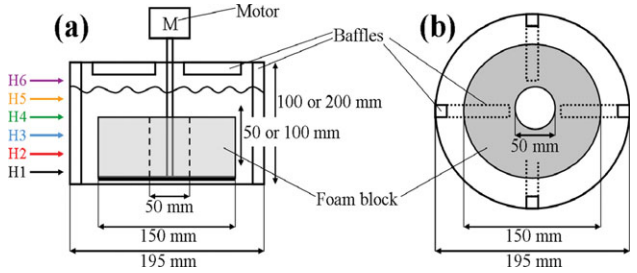

Figure 2. Schematical drawing of the rotating foam reactor (Reproduced from Ref. 16, with permission from Elsevier).

Side view with heights (a) and top view with baffles on top (b). [Color figure can be viewed in the online issue, which is available at wileyonlinelibrary.com.]

For more realistic conditions, tomography methods developed for the medical industry have been increasingly applied in the study of chemical reactors on the laboratory scale but also for pilot scale units.[19,20] Recently, Dudukovic and coworkers[21] have evaluated various methods regarding their application in field tomography.[21] These methods allow an easy visualization of the effect of the reactor design and the operational conditions on the gas–liquid distribution. However, so far no method can give fast measurements covering a large part of the reactor in combination with high local resolution. As an example, capacitance and resistance tomography are fast methods to study dynamic processes.[22–25] The spatial resolution is, however, poor compared to other techniques due to the distribution of the electric field between two electrodes. X-ray tomography is another fast technique with a high spatial resolution in the submillimeter range.[26] It provides detailed maps of the gas–liquid holdup in stirred tanks and trickle bed reactors.[7,27–32] The length of the penetration path limits the sample size to around 200 mm due to the absorption of X-rays in liquids. Additional calibration is needed due to beam hardening.[33]

γ-ray tomography has already been used to study the gas holdups in stirred tank reactors to validate CFD measurements.[30,31,34–37] Tomographic imaging techniques do not require any special preparation for the studied reactor system and give a good spatial resolution in the millimeter range. Isotopic sources are used having a much higher photon energy compared to sources used in commercially available X-ray Computer tomography (CT) systems for medical or nondestructive testing applications. Reactor walls can be made of denser material, which allows experiments at high-pressures. Additionally, isotopic sources offer discrete energy lines whereby the measurement accuracy can be increased by excluding scattered gamma photons from the measurement. This is not possible if X-ray sources are used, which generate polyenergetic spectra. Typical isotopic sources for tomographic applications are ^{241}Am (59.5 keV), ^{22}Na (511 keV), ^{137}Cs (662 keV), or ^{60}Co (1.17 MeV and 1.33 MeV). Depending on the isotopic source, different material thicknesses can be scanned and the contrast between the phases can be made visible. One main disadvantage of isotopic sources is the low photo flux. To achive a sufficient signal-to-noise ratio, radiation detectors have to be operated in counting mode. Because of this fact, the measurement time has to be large enough to collect a sufficient amount of photons at the radiation detector. Thus, a time averaged cross-sectional material distribution can be obtained from a CT scan. For gas holdup measurements inside the foam block this is sufficient, as we expect the gas holdup to change with the radius, but to be constant over the perimeter.

Table 1. Properties of the Used Liquids

Liquid	Concentration	Liquid density (g cm^{-3})	Dynamic Viscosity (mPa s)	Surface Tension (mN m^{-1})
Water	–	0.978	1	72.6
Water/glycerol	80/20 wt %	1.207	52	66.4
Glycerol	–	1.260	980	63.1

To determine the mean gas holdup, two additionally calibration CT scans have to be accomplished, one in which the reactor is completely filled with liquid (0% gas fraction) and one with no liquid inside (100% gas fraction).

In this study, γ-ray tomography was applied. Another important method is nuclear magnetic resonance imaging. It has been used extensively to study hydrodynamics in multiphase reactors, such as the occurrence of flooding in trickle bed reactors, but also moisture transport in concrete materials.[38–44]

Experimental

Rotating foam reactor

A schematic drawing of the rotating foam reactor is shown in Figure 2. All scanned reactor parts were built entirely of nonmetallic compounds to reduce the measurement time. A poly(methyl methacrylate) (PMMA) cylinder having an inner diameter of 195 mm, a thickness of 3 mm, and a height of 100 mm was used as reactor mantle. Top and bottom PMMA plates had a thickness of 30 mm. The reactor mantle and the reactor lid were equipped with four baffles with a thickness of 10 mm and a width of 10 mm to improve the mixing. As foam block stirrers, cylindrical shaped polypropylene foams with an inner diameter of 50 mm, an outer diameter of 150 mm and a height of 50 mm were used. The foam pore sizes were 10 and 20 linear ppi. A polyvinyl chloride (PVC) plate was used to fix the foam block. The plate was connected to a PVC stirrer shaft. Air was used as gas phase. As liquid phases water, a glycerol/water mixture of 80/20 wt % and pure glycerol were investigated. Properties of the liquids are found in Table 1. All measurements were performed at a temperature of 23°C, which was the temperature during the tomography experiments.

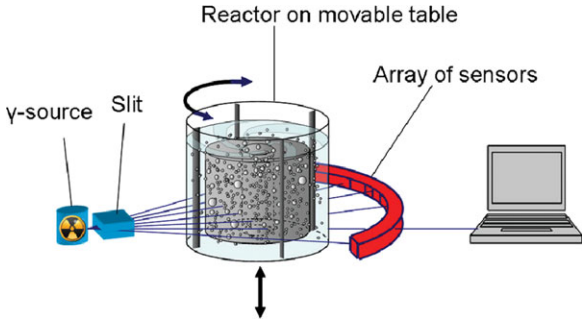

Figure 3. Principle of the γ-ray tomography, (Reproduced from Ref. 16, with permission from Elsevier).

The reactor is scanned under operation conditions at different heights. By rotating the object table, the gas holdup is resolved in 2-D at every height. [Color figure can be viewed in the online issue, which is available at wileyonlinelibrary.com.]

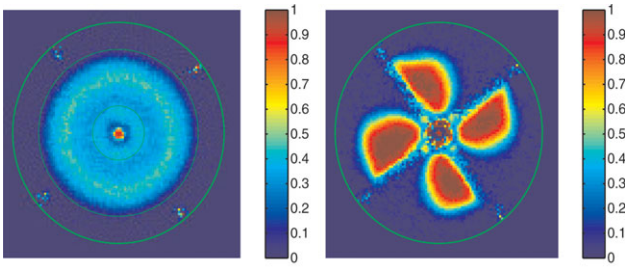

(a) 200 rpm, H2 (b) 200 rpm, H6

Figure 4. Tomographic images of the air/water mixture at the heights H2 and H6.

[Color figure can be viewed in the online issue, which is available at wileyonlinelibrary.com.]

The torque applied at various rotational speeds was measured using a Viscoklick VK 600.1 torque meter from IKA. From that the power input per liquid volume was calculated by

$$P_L = \frac{2\pi\tau\omega}{V_L} \quad [\mathrm{W\ m_L^{-3}}] \tag{1}$$

using the measured torque τ, the rotational speed ω, and the liquid volume V_L. The relative error due to the fluctuations of the torque was less than 3%.

Tomography measurements

The principle of the γ-ray CT system applied to the stirred reactor is shown in Figure 3. Technical details of the measurement system are described elsewhere.[45] As isotopic source ^{137}Cs with an activity of 180 GBq was used. The isotopic source was collimated to a 44° wide radiation fan beam and directed toward the radiation detector arc located approximately in a distance of 1 m. The detector arc contains 320 seamlessly arranged single detectors with an active area of 2 mm in width and 8 mm in height. The detector arc was vertically collimated to a slit height of about 2 mm by two lead arcs to reduce both the height of the volume segment to be analyzed and scattered radiation measurements. The reactor was installed on a rotational desk between γ-ray source and the radiation detector. During a measurement, the object table, the reactor was placed on, rotated continuously between the fixed ensemble of source and detectors with a speed of one rotation per 15 min. Thus, projection data is averaged over 10 rotations at a foam rotational speed of 200 rpm. It was experimentally confirmed that this was sufficient to assume a time averaged holdup measurement. Before the measurement, the zero height was defined to be the top part of the PVC plate supporting the foam block stirrer. The absorption due to the plate is stronger than in the solid foam. That position could easily be identified by moving the reactor up and downwards and measuring the absorption online. From that position, the reactor was moved downwards 6.5 mm, which indicated the first measuring plane H1. The planes H2 to H6 in Figure 2 were measured by moving the reactor downwards for distance of 13 mm resulting in six measurement heights for every operational mode. To determine the gas holdup, two calibration measurements had to be performed. For 100% gas holdup, the reactor was scanned with a dry foam, thus $\epsilon_G = 1$. For zero gas holdup, the reactor was flooded with liquid, so $\epsilon_G = 0$. In both cases, the reactor rotates with a rotational speed of 200 rpm. Subsequently, the liquid volume was adjusted to 2.0 L and the holdup measurements at rotational speeds between 150 and 300 rpm were performed. To obtain cross-sectional attenuation coefficient distributions, the standard algebraic reconstruction technique was used.[46] It utilizes the iterative correction formula

$$\mu_{i,j}^{(t+1)} = \mu_{i,j}^{(t)} + \lambda \frac{a_{i,j,p,d}\left(E_{p,d} - \sum_{i=0}^{n_x}\sum_{j=0}^{n_y} a_{i,j,p,d}\mu_{i,j}^{t}\right)}{\sum_{i=0}^{n_x}\sum_{j=0}^{n_y} a_{i,j,p,d}^2} \tag{2}$$

where n_y and n_x denote the dimensions of the attenuation data matrix, p and d the number of projections and detectors, E the attenuation data from measurements, and i and j denote indices of the corrected image pixel. a denotes the spatial overlap of a pixel with a given ray, wherein the pixel size was defined to be 2 mm by 2 mm. We used an iteration number $t = 10$. A relaxation factor λ of 0.01 was applied. This parameter may be tuned to improve convergence. The gas holdup was calculated using the reconstructed attenuation data of both calibration measurements as well as the gas holdup measurements

$$\epsilon_G = 1 - \frac{\mu_{i,j}^{\epsilon_G} - \mu_{i,j}^{\epsilon_G=1}}{\mu_{i,j}^{\epsilon_G=0} - \mu_{i,j}^{\epsilon_G=1}} \quad [\mathrm{m_G^3\ m_{G+L}^{-3}}] \tag{3}$$

Representive tomography images of the gas holdup inside the foam block as well as above the block derived from the measurements can be found in the Figures 4 and 5.

Results and Discussion

Effect of pore size

In the case of a rotating foam reactor and using water as working fluid, the Power number is constant in the range of rotational speeds investigated. A similar power input means

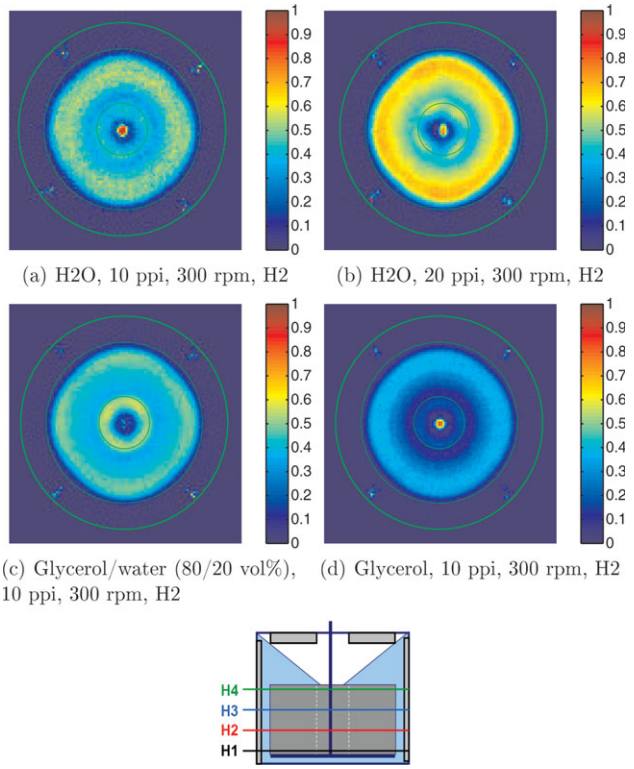

(a) H2O, 10 ppi, 300 rpm, H2 (b) H2O, 20 ppi, 300 rpm, H2

(c) Glycerol/water (80/20 vol%), 10 ppi, 300 rpm, H2 (d) Glycerol, 10 ppi, 300 rpm, H2

Figure 5. Tomographic images of water, a glycerol/water mixture and glycerol at height H2; rotational speed 200 and 300 rpm; gas phase air; foam pore sizes 20 ppi and 10 ppi.

[Color figure can be viewed in the online issue, which is available at wileyonlinelibrary.com.]

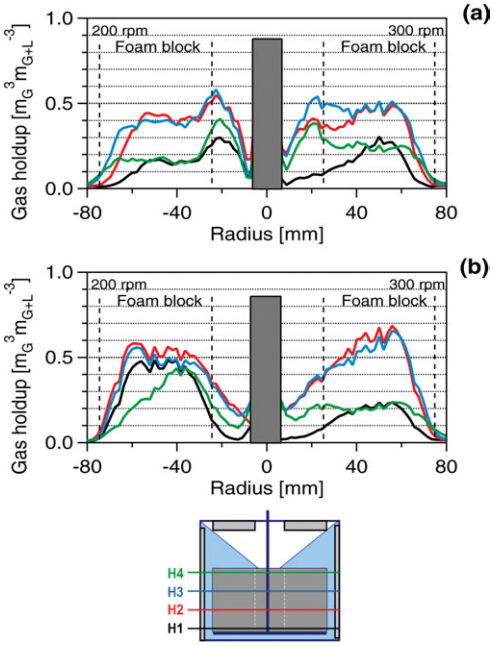

Figure 6. Radial gas holdup profiles for a polypropylene foam with a pore size of 10 ppi (a) and 20 ppi (b) at the positions H1 to H4 for water; rotational speed 200 and 400 rpm; gas phase is air.

[Color figure can be viewed in the online issue, which is available at wileyonlinelibrary.com.]

that the pressure drop over the bed is comparable and the liquid velocity is reduced compared to larger pores. In general, the energy dissipation consists of three parts: (i) flow through the foam block, section B; (ii) backflow to the reactor center, section C to A; (iii) turbulence in the outer reactor volume, section C. In Figure 8b, the inflow velocity of liquid is shown, assuming that the energy applied to the system is entirely consumed by the flow through the foam block. The two-phase pressure drop was calculated using the solid foam properties given in Table 2.[16] Because of energy dissipation in the remaining reactor volume, especially at the baffles, the actual velocity is lower than that value. The centrifugal forces on the liquid in the foam block is, however, the main driving force for liquid flow. Using a solid foam block, the power input would be very low. Figure 8b gives, thus, a reasonable estimate of the order of magnitude of the liquid circulation velocity. Using a 20 ppi foam block, Figure 8b shows a theoretical liquid inflow velocity, which is two third of the value for the 10 ppi foam block. Further, the penetration of bubbles through the smaller pores is hindered and the bubbles are easier trapped inside the solid foam cells. This effect leads to a high gas holdup in the Figures 5 and 6. Holdup values exceeding 0.5 m^3_G m^{-3}_{G+L} are found. Such a high holdup results eventually in coalescence of bubbles. After stopping the stirrer, bubbles leaving the foam block on top with sizes of more than 10 mm have been observed, while the foam cell size is around 3 mm. This results in dry sections of the foam block, which do not contribute to the mass transfer and reaction rate. Further, the cross-sectional area available for the liquid flow is reduced. This reduced the cross-sectional area for liquid flow through the foam block and the flow rate. As a result, the gas holdup in the reactor section C between foam block stirrer and reactor mantle is also reduced (Figure 7a). Visual observations have shown that the bubble size for both pore sizes is less than 2 mm for a rotational speed of 200 rpm. Using higher rotational speeds for the 10 ppi foam block larger bubbles of up to 5 mm are formed by coalescence at higher gas holdups. For the 20 ppi foam, the bubble size is still less than 2 mm even at high rotational speeds of 300 rpm. In the outer section C, using water, the flow can be characterized as turbulent. As the Reynolds number is larger than $1.2{\cdot}10^4$, the Power number is independent of the rotational speed and depends only on reactor design and the liquid density. Both foam block stirrers have the same dimensions. As a result, the Power number is constant over the entire range of measured rotational speeds, as shown in Figure 8a.[47] Additional energy is dissipated by the flow through the foam pores. The radial forces are excerted on the same liquid volume due to a similar bed porosity and comparable gas holdups. The energy dissipation per bed volume is, therefore, also comparable.

Assuming the liquid velocities shown in Figure 8 for 300 rpm, the Reynolds number inside the foam block based on the strut diameter is around 420 for the 10 ppi foam and 180 for the 20 ppi foam (Table 3). The flow can be described in the laminar regime, but not vortex free. For Reynolds numbers higher than 50, the flow past cylinders forms Karman vortex streets.[48]

We can summarize, that the reduction of the solid foam pore size results in a reduced liquid circulation velocity. The mixing of gas and liquid in the center section is reduced and fewer bubbles are transported through the foam block to the outer reactor section. A large number of these bubbles entering the foam block is trapped inside the solid foam cells, which increases the pressure drop even more.

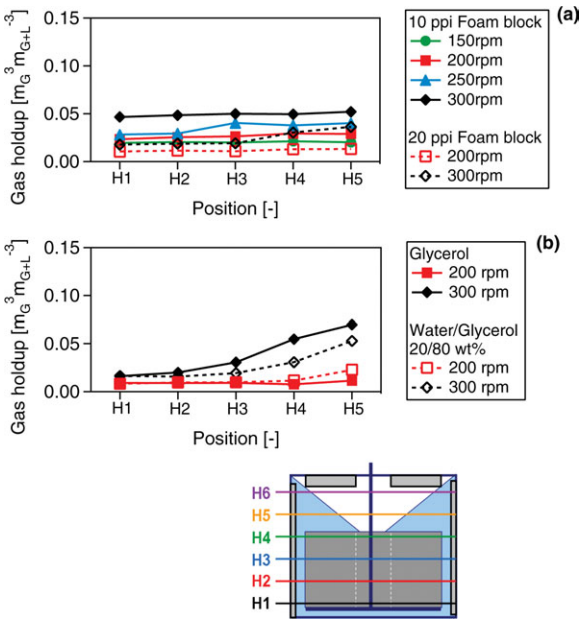

Figure 7. Gas holdup profiles in the outer reactor section between foam block and reactor wall at the heights H1 to H5 for water using 10 ppi and 20 ppi foam pore size (a) and glycerol and glycerol/water (80/20 vol %) using a 10 ppi foam (b).

[Color figure can be viewed in the online issue, which is available at wileyonlinelibrary.com.]

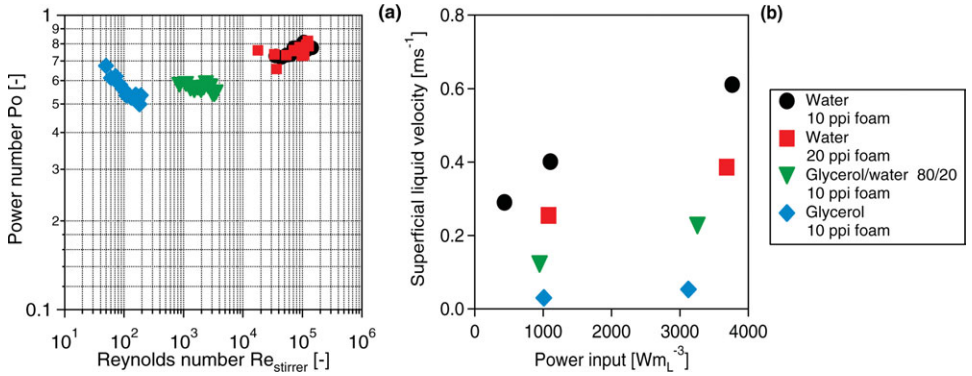

Figure 8. Power number depending on Stirrer Reynolds number (a) and theoretical velocity of liquid through the foam structure depending on the power input (b).

[Color figure can be viewed in the online issue, which is available at wileyonlinelibrary.com.]

We can now relate this to the mass transfer performance. The gas–liquid mass transfer depends on the gas holdup, the bubble size, and further on the refreshment rate of the gas liquid interface. All three parameters are directly related to the velocity of liquid circulation. Using a 20 ppi foam block, the low liquid inflow velocity reduce the mixing and the gas holdup in the center section around the stirrer shaft. This results in both lower k_{GL}- and a_{GL}-values. A slow liquid flow through the foam block passing the trapped bubbles results additionally in lower k_{GL}-values. In the outer section, the gas holdup and therewith the a_{GL}-value is reduced as well (Figure 7a). The k_{GL} value in that section should be similar to the 10 ppi foam, as long as bubble coalescence in the foam block pores is not significant. Consequently, we find that the gas–liquid mass transfer is reduced with smaller pore size, which is in agreement with values obtained for the absorption of oxygen into water.[14]

The liquid–solid mass transfer rate depends on the geometric surface area of the foam block and on the relative velocity between liquid and solid. A smaller pore size results in higher liquid–solid interfacial area. Considering the foam block structure only, a 10 ppi foam has a specific surface area of around 500–600 m^2 m^3, while using a 20 ppi foam the value is 900–1000 m^2 m^3 (Table 2). This is, however, counterbalanced by the reduced liquid velocities, shown in Figure 8b. In earlier measurements, we found that the $k_{LS}a_{LS}$-value is around one third higher using a 20 ppi foam block compared to a 10 ppi foam block. The higher pressure drop does not completely counterbalance the interfacial area and a smaller pore size is beneficial. Even smaller pore sizes would result to even lower liquid circulation. Next to the increased bubble entrapment, also practical difficulties concerning catalyst deposition would arise. Smaller pore sizes are, therefore, only beneficial, if the gas–liquid mass transfer is sufficiently high and the process is liquid–solid mass transfer limited, catalyst pore diffusion limited or kinetically limited.

Table 2. Foam Block Characteristics

ppi Number	Foam Pore Diameter* (mm)	Foam Cell Diameter* (mm)	Strut Thickness* (mm)	Specific Surface Area† [m^2_{LS} m^{-3}_{Bed}]
10	2–4	4–7	0.6	580
20	1–2	2–4	0.3	960

*Measured.
†Calculated using correlations of Fourie and Du Plessis.[53]

Effect of viscosity

To study the influence of viscosity using a Newtonian liquid, the gas holdup for water was compared to a 80:20 wt % mixture of glycerol and water and pure glycerol. The properties of the measured liquids are listed in Table 1. The values agree well with literature data.[49–51] The viscosity increases strongly with the glycerol concentration. The surface tension is also reduced compared to pure water. As already discussed in the previous section, using water in combination with a 10 ppi foam, the liquid velocity through the foam block pores is in the range of 0.2–0.6 ms^{-1}. As the liquid flows into the center section above the foam block, it is mixed with gas. The produced bubbles are then transported through the foam. Regarding the gas holdup, at low rotational speeds of 200 rpm, strong differences can be found depending on the viscosity. Using the 80:20 wt % mixture of glycerol and water, the viscosity is increased 80 times. This results in a strong reduction of the liquid circulation velocity through the foam block. Theoretical values less than 50% compared to water are found in Figure 8. In the center section between foam block and stirrer shaft, still a high average gas holdup is found, which is similar to water. This can be explained by two effects. First, the liquid inflow into this section is still high enough to achieve a sufficient formation and break up of bubbles. Additionally, the reduced surface tension improves the bubble breakup. In this case of glycerol/water, the gas holdup in the center section is strongly reduced moving from height H4 to H2 (Figure 9a). As a comparison, for water the holdup is relatively uniform over the heights H2 to H4 (Figure 6a). Further, the gas holdup inside the foam block is reduced. This can be interpreted that significantly larger bubbles are formed, compared to water. These accumulate in the top part of this section close to the stirrer shaft and gas–liquid interface, which was also observed visually. A similar profile has been obtained investigating the gas holdup of non-Newtonian liquids with a comparable viscosity.[16] The volumetric flow rate into the foam block is too slow to transport the bubbles.

Table 3. Reynolds Numbers Based on the Stirrer and Strut Diameter

Liquid	ppi	$Re_{stirrer}$ at 300 rpm	Re_{strut} at 300 rpm
Water	10	10^5	413
Water	20	10^5	175
Water/glycerol	10	2600	1.9
Glycerol	10	150	0.026

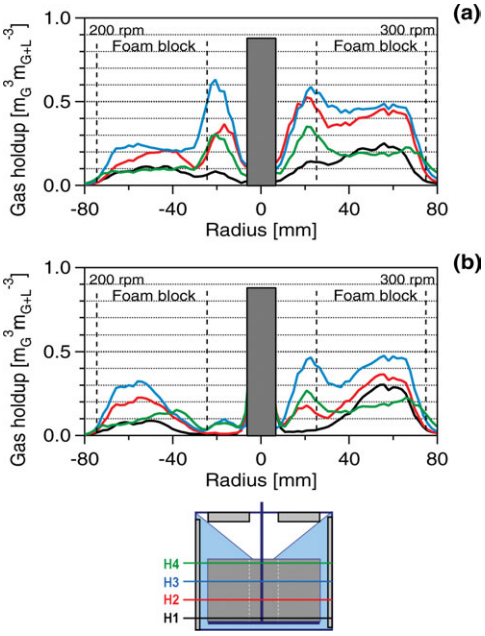

Figure 9. Radial gas holdup profiles for a polypropylene foam at positions H1 to H4 for a mixture of glycerol and water (80/20 vol %) (a) and glycerol (b); rotational speed 200 and 300 rpm; gas phase air.

[Color figure can be viewed in the online issue, which is available at wileyonlinelibrary.com.]

The use of pure glycerol results in an even lower liquid circulation. Figure 8b shows that the velocity through the solid foam cells is in the order of centimeters per second. This low circulation velocity results in a low liquid inflow into the center section and a low gas holdup in the section between stirrer shaft and foam block. Thus, the gas holdup inside the foam block is low, even in the top part of the foam block (H4 in Figure 9a).

At a rotational speed of 300 rpm, the average gas holdup increases with the rotational speed for all liquids and the gas holdup in the center section around the stirrer shaft and the foam block becomes more uniform. The holdup profile for the glycerol/water mixture becomes similar to water (Figures 6a and 9b). For pure glycerol, the profile shows a lower uniformity over the radius (Figure 9b). Comparing different reactor heights, a gradient is still visible.

Figure 8a shows that for the glycerol/water mixture, the Power number is still independent of the Reynolds number, the latter being in the range of 10^3. The flow dynamics in the outer reactor section between foam block and reactor mantle can still be described as turbulent, but already close to the transition regime between laminar and turbulent flow. For glycerol, the Reynolds number has values between 50 and 200. This is clearly in the laminar regime and, thus, the Power number becomes dependent on the Reynolds number (Figure 8a).

Regarding the gas holdup in the outer section between foam block and reactor wall, a trend similar to the reactor volume around the stirrer shaft is found. For the pure water system, the gas holdup is uniform over the heights H1 to H5. With increasing viscosity, the gradient develops. For pure glycerol, the gas holdup at height H5 even exceeds the holdup for water. This suggests that the bubbles in this reactor section are mainly produced at the baffles at the reactor lid. They are not transported through the foam block but remain in the reactor section above the foam block.

Concerning the mass transfer rates, this has several consequences. As the viscosity increases, the Reynolds number is reduced. Further the diffusion coefficient and the k_{GL} value are reduced. Additionally, as already discussed, the gas liquid mass transfer becomes more and more localized to the top part of the reactor. The lower reactor part is, therefore, not significantly contributing to the gas–liquid mass transfer. At higher viscosity, the gas–liquid mass transfer inside the foam block occurs mainly between immobilized bubbles and the passing liquid. With a low liquid velocity and a high viscosity, the k_{GL}-value is reduced, consequently.

Similar conclusions can be drawn for the liquid–solid mass transfer. The k_{LS}-value is reduced with the diffusion coefficient using higher viscosity, and further by the reduced velocity of liquid passing the foam block struts.[52]

Comparing the Reynolds numbers based on the strut diameter in Table 3, we find that already for the glycerol/water mixture the Reynolds number is two orders of magnitude lower compared to water. The flow passing the struts is, thus, laminar and vortex free and no mass transfer enhancement due to the flow around the struts is found. To improve the liquid flow at higher viscosities, a larger pore size needs to be used. This would increase the liquid circulation rate and the Reynolds number inside the foam pores, but would also reduce the liquid–solid interfacial area.

Concluding Remarks

γ-ray tomography measurements give a detailed picture of the local gas holdup, from which conclusions can be drawn on the hydrodynamics and the mass transfer of rotationg foam reactors.

The foam block stirrer investigated is especially interesting for liquids having a viscosity of less than 50 mPas. The flow passing the struts can be characterized as laminar, but showing vortices, which results in high liquid–solid mass transfer rates. At lower pore sizes, the liquid–solid interfacial area increases, but reduces liquid circulation. This leads to bubble entrapment in the foam block and a reduced gas holdup in the remaining reactor volume, especially in the center section around the stirrer shaft. Using medium foam block pore sizes of 10 to 20 ppi, the trade off between these phenomena results in a high liquid flow velocity through the pores in the order of decimeters per second. Using higher viscosity, the liquid circulation through the foam block is strongly reduced. The flow passing the struts is vortex free and the bubble formation rate is strongly reduced. Significant gas holdups are found only in the upper reactor part. To use the entire reactor volume efficiently, the rotational speed can be increased. This would increase the liquid circulation and a more homogeneous gas holdup over the height. Other adjustments can be done on the design of the reactor and foam block. For higher viscosities, the foam block pore size can be increased to reduce the pressure drop and increase the liquid circulation. An important point is the design of foam block and reactor. As the bottom part does not sufficiently take part in the mass transfer process, the foam block thickness in this part should be reduced, for example, using a conical foam block shape. Further, the distance between foam block and reactor bottom should be increased to allow the liquid also circulate below the foam block and not only above. The baffle design can be optimized to improve the liquid flow into the center section.

Acknowledgments

Financial support by the Dutch Technology Foundation STW is gratefully acknowledged.

Notation

$a_{i,j,p,d}$ = spatial overlap between pixel and array
a_{GL} = specific gas–liquid interfacial area, $m^2_{GL}\ m^{-3}_L$
k_{GL} = gas–liquid mass-transfer coefficient, m s^{-1}
a_{LS} = specific liquid–solid interfacial area, $m^2_{LS}\ m^{-3}_L$
k_{LS} = liquid–solid mass-transfer coefficient, m s^{-1}
$D_{stirrer}$ = stirrer diameter, m
D_{strut} = average foam strut diameter, m
E = attenuation
P = power input, W
P_L = power input per liquid volume, W m^{-3}_L
$Po = \frac{P}{\rho\omega^3 d^5}$ = Power number, W m^{-3}_L
$Re_{stirrer} = \frac{\rho u_L D_{stirrer}}{\mu}$ = stirrer Reynolds number
$Re_{strut} = \frac{\rho u_L D_{strut}}{\mu}$ = strut Reynolds number
rpm = rotational speed, min^{-1}
t = iteration step
u_L = superficial liquid velocity, m s^{-1}
V_L = liquid volume, m^3

Greek letters

ϵ_G = gas holdup, $m^3_G\ m^{-3}_{G+L}$
λ = relaxation factor
μ = dynamic viscosity, Pa s
$\mu_{i,j}$ = attenuation coefficient
ρ = density, g cm^{-3}
τ = applied torque, N m
ω = rotational speed, s^{-1}

Indices

d = number of detectors
i, j = indices of the corrected image pixel
p = number of projections

Literature Cited

1. Albers RKE, Houterman MJJ, Vergunst T, Grolman E, Moulijn JA. Novel monolithic stirred reactor. *React Kinet Catal Lett*. 2004;44: 2459–2464.
2. De Greef J, Desmet G, Baron G. Micro-fiber elements as perfusive catalysts or in catalytic mixers: flow, mixing and mass transfer. *Catal Today*. 2005;105:331–336.
3. Hoek I. Towards the Catalytic Application of a Monolithic Stirrer Reactor. Ph.D thesis, TU Delft, The Netherlands, 2004.
4. Pletcher D, Whyte I, Walsh FC, Millington JP. Reticulated vitreous carbon cathodes for metal ion removal from process streams part I: mass transport studies. *J Appl Electrochem*. 1991;21:659–666.
5. Edouard D, Lacroix M, Pham C, Mbodji M, Pham-Huu C. Experimental measurements and multiphase flow models in solid SiC foam beds. *AIChE J*. 2008;54:2823–2832.
6. Hutter C, Zenklusen A, Lang R, Rudolf von Rohr P. Axial dispersion in metal foam and streamwise-periodic porous media. *Chem Eng Sci*. 2011;66:1132–1141.
7. Calvo S, Beugre D, Crine M, Leonard A, Marchot P, Toye D. Phase distribution measurements in metallic foam packing using X-ray radiography amd micro-tomography. *Chem Eng Process*. 2009;48: 1030–1039.
8. Stemmet C, van der Schaaf J, Kuster BFM, Schouten JC. Solid foam packings for multiphase reactors: Modelling of liquid holdup and mass transfer. *Chem Eng Res Des*. 2006;84:1134–1141.
9. Keyvani M, Gardner NC. Operating characteristics of rotating beds. *Chem Eng Progress* 1989;9:48–52.
10. Munjal S, Dudukovic MP, Ramachandran P. Mass-transfer in rotating packed beds-II. Experimental results and comparison with theory and gravity flow. *Chem Eng Sci*. 1989;44:2257–2268.
11. Lin CC, Jian GS. Characteristics of a rotating packed bed equipped with blade packings. *Sep Purif Technol*. 2007;54:51–60.
12. Dhiman SK, Verma V, Rao DP, Rao MS. Process intensification in a trickle-bed reactor: experimental studies. *AIChE J*. 2005;51: 3186–3192.
13. Burns JR, Ramshaw C. Process intensification: visual study of liquid maldistribution in rotating packed beds. *Chem Eng Sci*. 1997;52: 455–460.
14. Tschentscher R, Njhuis TA, van der Schaaf J, Kuster BFM, Schouten JC. Gas-liquid mass transfer in rotating solid foam reactors. *Chem Eng Sci*. 2010;65:472–479.
15. Tschentscher R, Njhuis TA, van der Schaaf J, Schouten JC. Liquid-solid mass transfer in agitated slurry reactors and rotating solid foam reactors. *Ind Eng Chem Res*. 2010;49:10758–10766.
16. Tschentscher R, Schubert M, Bieberle A, Nijhuis TA, van der Schaaf J, Hampel U, Schouten JC. Tomography measurements of gas holdup in rotating foam reactors with Newtonian, non-Newtonian and foaming liquid. *Chem Eng Sci*. 2011;66:3317–3327.
17. Boyer C, Duquenne AM, Wild G. Measuring techniques in gas-liquid and gas-liquid-solid reactors. *Chem Eng Sci*. 2002;57:3185–3215.
18. Bucharsky EC, Schell KG, Oberacker R, Hoffmann MJ. Preparation of transparent glass sponges via replica method using high-purity silica. *J Am Ceram Soc*. 2010;93:111–114.
19. Al-Dahhan MH, Kemoun A, Cartolano AR. Phase distribution in an upflow monolith reactor using computed tomography. *AIChE J*. 2006;52:745–753.
20. Al-Dahhan MH, Kemoun A, Cartolano R, Roy S, Dobson R, Williams J. Measuring gas–liquid distribution in a pilot scale monolith reactor via an industrial tomography scanner (ITS). *Chem Eng J*. 2007;130:147–152.
21. Kuzeljevic Z, Dudukovic M, Stitt H. From laboratory to field tomography: data collection and performance assessment. *Ind Eng Chem Res*. 2011;50:9890–9900.
22. Hamidipour M, Larachi F. Dynamics of filtration in monolith reactors using electrical capacitance tomography. *Chem Eng Sci*. 2010;65:504–510.
23. Hui LK, Bennington CPJ, Dumont GA. Cavern formation in pulp suspensions using side entering axial-flow impellers. *Chem Eng Sci*. 2009;64:509–519.
24. Mann R, Wang M, Forrest AE, Holden PJ, Dickin FJ, Dyakowski T, Edwards RB. Gas-liquid and miscible liquid mixing in a plant-scale vessel monitored using electrical resistance tomography. *Chem Eng Commun*. 1999;175:39–48.
25. Wang M, Dorward A, Vlaev D, Mann R. Measurements of gas-liquid mixing in a stirred vessel using electrical resistance tomography. *Chem Eng J*. 2000;77:93–98.
26. Bieberle M, Fischer F, Schleicher E, Koch D, Menz HJ, Mayer HG, Hampel U. Experimental two-phase flow measurement using ultra fast limited-angle-type electron beam X-ray computed tomography. *Exp Fluids* 2009;49:369–378.
27. Boden S, Hampel U, Bieberle M. Measurement of gas hold-up distribution in a stirred chemical reactor using X-ray cone-beam computed tomography. *Chem Eng J*. 2008;139:351–362.
28. Ford JJ, Heindel TJ, Jensen TC, Drake JB. X-ray computed tomography of a gas-sparged stirred-tank reactor. *Chem Eng Sci*. 2008;63:2075–2085.
29. Heindel TJ, Gray JN, Jensen TC. An X-ray system for visualizing fluid flows. *Flow Meas Instrum*. 2008;19:67–78.
30. Thatte AR, Ghadge RS, Patwarhan AW, Joshi JB, Singh G. Local gas holdup measurement in sparged and aerated tanks by γ-ray attenuation technique. *Ind Eng Chem Res*. 2004;43:5389–5399.
31. Kopkar AR, Rammohan AR, Ranade VV, Dudukovic MP. Gas-liquid flow generated by a Rushton turbine in stirred vessel: CARP/CT measurements and CFD simulations. *Chem Eng Sci*. 2005;60:2215–2229.
32. Hubers JL, Striegel AC, Heindel TJ, Gray JN, Jensen TC. X-ray computed tomography in large bubble columns. *Chem Eng Sci*. 2005;60:6124–6133.
33. Hampel U, Hristov HV, Bieberle A, Zippe C. Application of high-resolution gamma ray tomography to the measurement of gas holdup distributions in a stirred chemical reactor. *Flow Meas Instrum*. 2007;18:184–190.
34. Hristov HV, Boden S, Hampel U, Kryk H, Hessel G, Schmitt W. A study on the two-phase flow in a stirred tank reactor agitated by a gas–inducing turbine. *Chem Eng Res Des*. 2008;86:75–81.
35. Jin H, Yang S, Guo Z, He G, Tong E. The axial distribution of holdups in an industrial-scale bubble column with evaluated pressure using γ-ray attenuation approach. *Chem Eng J*. 2005;115:45–50.
36. Kumar SB, Moslemian D, Dudukovic MP. A γ-ray tomographic scanner for imaging voidage distribution in two-phase flow systems. *Flow Meas Instrum*. 1995;6:61–73.
37. Veera UP, Joshi JB. Measurement of gas hold-up profiles in bubble column by gamma ray tomography. *Chem Eng Res Des*. 2000;78:425–434.
38. van der Heijden GHA, Huinink HP, Pel L, Koping K. Non-isothermal drying of fired-clay brick, an NMR study. *Chem Eng Sci*. 2009; 64:3010–3018.

39. Gladden LF, Anadon LD, Lim MHM, Sederman AJ, Stitt EH. Insights into the mechanism of the trickle-to-pulse transition in trickle-bed reactors. *Ind Eng Chem Res*. 2005;44:6320–6331.
40. Heibel AK, Vergeldt FJ, van Ass H, Kapteijn F, Moulijn JA, Boger T. Gas-liquid distribution in the monolith film flow reactor. *AIChE J*. 2003;49:3007–3017.
41. Daidzic NE, Schmidt E, Hazan MM, Altobelli S. Gas-liquid phase distribution and void fraction measurements using MRI. *Nucl Eng Des*. 2005;235:1163–1178.
42. Harel E, Hilty C, Koen K, McDonnell EE, Pines A. Time-of-flight imaging of two-phase mixing inside a microfluidic chip. *Phys Rev Lett*. 2007;98:017601–017604.
43. Stapf S, Han S-I. *NMR Imaging in Chemical Engineering*. Weinheim, Germany, Wiley-VCH, 2006.
44. Gladden LF. Recent advances in MRI studies of chemical reactors: ultrafast imaging of multiphase flows. *Top Catal*. 2003;24:19–24.
45. Hampel U, Bieberle A, Hoppe D, Kronenberg J, Schleicher E, Suehnel T, Zimmermann F, Zippe C. High resolution gamma ray tomography scanner for flow measurement and non-destructive testing applications. *Rev Sci Instrum*. 2007;78103704–78103712.
46. Kak AC, Slaney M. *Principles of Computerized Tomographic Imaging*. Philadelphia: Society of Industrial and Applied Mathematics, 2001.
47. Sanchez Perez JA, Rodrigues Porcel EM, Casas Lopez JL, Fernandez Sevilla JM, Christi Y. Shear rate in stirred tank and bubble column bioreactors. *Chem Eng J*. 2006;124:1–5.
48. Taneda S. Experimental Investigation of the wakes behind cylinders and plates at low Reynolds numbers. *J Phys Soc Jpn*. 1956;11:302–307.
49. Shankar PN, Kumar M. Experimental determination of the kinematic viscosity of glycerol-water mixtures. *Proc R Soc London A*. 1994; 444:573–581.
50. Chenlo F, Moreira R, Pereira G, Bello B. Kinematic viscosity and water activity of aqueous solutions of glycerol and sodium chloride. *Eur Food Res Technol*. 2004;219:403–408.
51. Segur JB, Oberstar HE. Viscosity of glycerol and its aqueous solutions. *Ind Eng Chem Res*. 1951;43:2117–2120.
52. Huu TT, Lacroix M, Huu CP, Schweich D, Edouard D. Towards a more realistic modeling of solid foam: use of the pentagonal dodecahedron geometry. *Chem Eng Sci*. 2009;64:5131–5142.
53. Fourie JG, Du Plessis JP. Pressure drop modelling in cellular metallic foams. *Chem Eng Sci*. 2002;57:2781–2789.

Manuscript received Sept 20, 2011, revision received Jan. 29, 2012.